Chapter IV

Photoemission Final-State Effect on Electronic Properties of CdSe Nanocrystals

***Overview of the chapter*:**

Size-dependent energy shift of synchrotron photoemission spectra in the core level and valence-band edge, with respect to bulk sample, was reported for organics-passivated CdSe nanocrystals ranging in size from 18 to 42 Å. We attribute this shift to the photoemission final-state effect, which is characterized by a simple model based on an electrostatic calculation. For TOPO/HDA-passivated nanocrystals, the core-level shifts are well described with a model involving the static final-state effect, while an additional effect of the initial state due to quantum confinement is required to elucidate the energy shift of the valence-band edge. After the nanocrystals are treated with pyridine, the energy shifts are smaller; this decrease is ascribed to the dynamic final-state effect describing a finite lifetime, on a femtosecond scale, of the photohole residing in the nanoparticle. This condition is intimately related to the coupling between the nanoparticle and metallic substrate and among nanocrystals themselves.

4.1 Introduction

Photoemission spectroscopy is a powerful tool to investigate the electronic structure of nanomaterials [1,2]. The electron energy measured in a photoemission experiment is, in principle, influenced by effects in both the initial and final states. The initial-state effect is related to the intrinsic electronic properties of materials, while the final-state effect is ascribed to the photohole in the final state and the possible interaction between the outgoing electron and the positively charged state left behind. This charging effect in the final state is related to a quantum phenomenon in single-electron tunneling.

The final-state effect in photoemission spectra of small particles was first identified on Au clusters supported on poorly conducting substrates [3]. Subsequent investigations confirm and find more detailed information [4,5]. This final-state effect is also important to the ionization and affinity energies of metal clusters. Many calculations have been developed to describe these properties [6-8]. Recently, a simple dynamic model that takes into account the finite lifetime of the photohole provides a quantitative interpretation for the photoemission spectra of organics-passivated metallic clusters near the Fermi level; furthermore, the magnitude of the lifetime has been found to depend on the interaction between cluster and substrate [5,9-11].

For semiconductor NCs, in contrast, a detailed investigation of the energy shift, dependent on size, of core-level and valence-band photoemission spectra is lacking. In their pioneer work Colvin *et al*. discussed the relative energy shift of the valence-band maximum among CdS NCs [1]. Other authors subsequently concentrated on the quantum shift, relative to the bulk, of the initial state in the

valence-band edge by subtracting the core-level shift [12]. In order to reduce the problem of charging, NCs of thickness less than one monolayer on substrates were used in that work. Here, we are motivated by the size-dependent electronic properties of quantum-confined semiconductor NCs. By means of synchrotron, high-resolution PES, we are able to systematically explore the core-level and the valence-band spectra of CdSe NCs in detail. The effect of the interparticle coupling was also investigated.

4.2 Size dependence of high-resolution photoemission spectra

4.2.1 *TOPO/HDA-passivated CdSe nanocrystals*

a). Cd $3d_{5/2}$ and Se $3d$ core-level spectra

Figure 4.1 shows the Cd $3d_{5/2}$ and Se $3d$ core-level photoemission spectra of bulk CdSe and CdSe NCs, with three mean diameters (D_m) of 42, 32, and 18 Å, as well as the corresponding fits at room temperature. A polynomial background of these spectra was subtracted before fitting the features to the minimum number of Voigt functions.

All Cd $3d_{5/2}$ spectra, measured with a photon energy of 480 eV, can be satisfactorily fitted with a single Voigt function, despite the surface component should be pronounced due to the slightly rich Cd atoms at the NC surface (discussed in Chap. III). Therefore, we suppose the surface components of the Cd $3d_{5/2}$ spectra cannot be differentiated in energy, that is, Cd−O/N and Cd−Se have roughly the same binding energy. The spectrum of bulk solids shows a

binding energy of 405.6 eV, in agreement with a value reported in the literature [13]. For NC samples the Cd $3d_{5/2}$ spectra are shifted toward higher binding energy relative to the bulk crystallite. These spectra notably exhibit line broadening resulting from a finite distribution of size and an increased structural disorder [14,15].

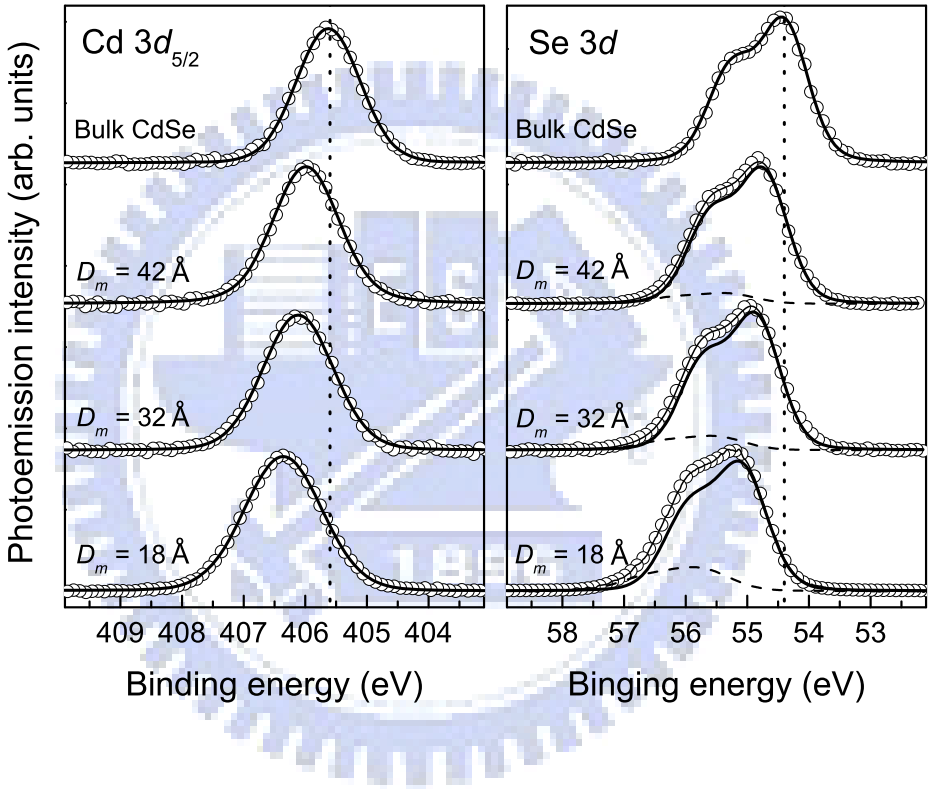

FIG. 4.1: Size-dependent Cd $3d_{5/2}$ and Se $3d$ photoemission spectra of bulk CdSe and TOPO/HDA-passivated CdSe nanocrystals, with three mean diameters (D_m), were measured at room temperature with photon energies of 480 eV and 120 eV, respectively. All Cd $3d$ spectra show good fits by only one single component (thick solid lines), whereas with the exception of bulk CdSe the Se $3d$ spectra of nanocrystal samples are composed of interior (thick solid lines) and surface components (dashed lines). The binding energies of the Cd $3d_{5/2}$ and Se $3d_{5/2}$ spectra of bulk sample are indicated.

The Se $3d$ core-level spectra were taken at a photon energy of 120 eV; to probe the same depth of the samples, this energy was chosen to obtain a kinetic

energy similar to that in the Cd $3d_{5/2}$ core-level spectra. A satisfactory fit was achieved with one single spin-orbit split doublet of Voigt function for the bulk sample. The obtained Se $3d_{5/2}$ feature has a binding energy of 54.4 eV, consistent with the literature value [16]. In contrast, two spin-orbit split doublets of Voigt functions were necessary to obtain fits of reliable quality for all Se 3*d* core-level spectra of the NC samples. The intensity of the component with higher binding energy increases relative to that of the other component as the particle size decreases. The component at higher binding energy is thus assigned to the surface Se atoms of CdSe NCs because the ratio of surface to bulk atoms is increasing with a reduction in particle size, while the other component arises from interior Se atoms. Our EXAFS studies, discussed in Chapter III, indicate that the surface Se atoms of as-prepared CdSe NCs are not bonding to the surfactants. Consequently, the surface component of the Se 3*d* core-level spectra that exhibits a chemical shift is due to unsaturated bonds, which will not be discussed here. In contrast, the interior Se 3*d* component has no chemical shift but shows a clear shift to higher binding energy relative to bulk CdSe, with the magnitude of the energy shift comparable to that of the Cd $3d_{5/2}$ core-level spectra.

b). Valence-band spectra

Figure 4.2 shows valence-band photoemission spectra of the same samples as represented in Fig. 4.1, measured at a photon energy 50 eV so as to have the same probing depth. We verified that the organic compounds contribute to the spectral region below about 5 eV, hence the first features below the valence-band edge are due purely to NC. On extrapolating the linear part just

below the edge to its intersection with a linear background, we determined the valence-band edge. For the NC samples the valence-band edges exhibit shifts towards binding energy greater than for the spectrum of a bulk sample. It is important to note that the energy shifts of the valence-band edge are always larger than those of the core levels especially for the smaller NCs, indicating a non-negligible difference in shifts between the valence-band edge and core levels.

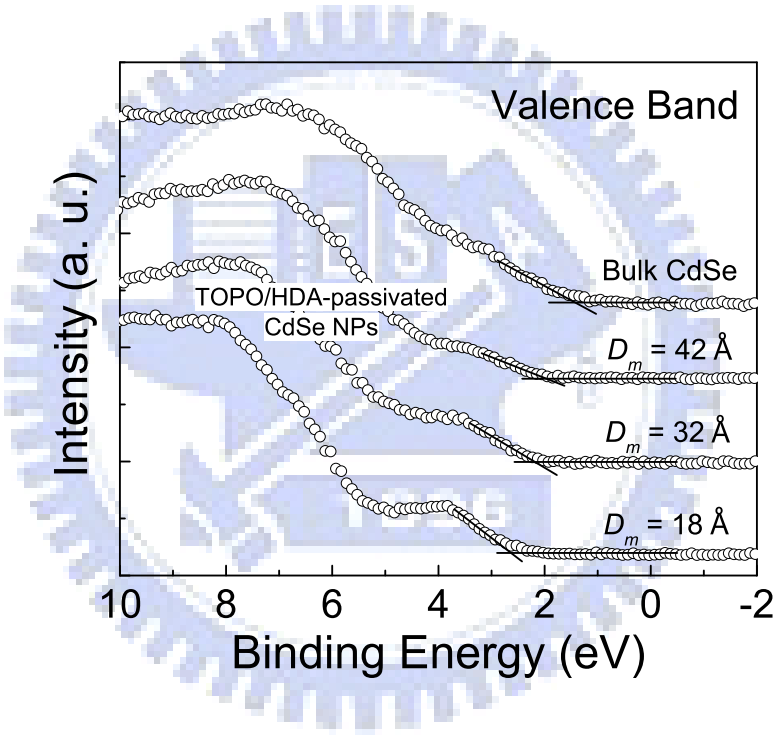

FIG. 4.2: Valence-band photoemission spectra of bulk CdSe and TOPO/HDA-passivated CdSe nanocrystals with three mean diameters (D_m) measured at a photon energy of 50 eV at room temperature.

4.2.2 *Pyridine-treated CdSe nanocrystals*

a). Core-level spectra of organic ligands

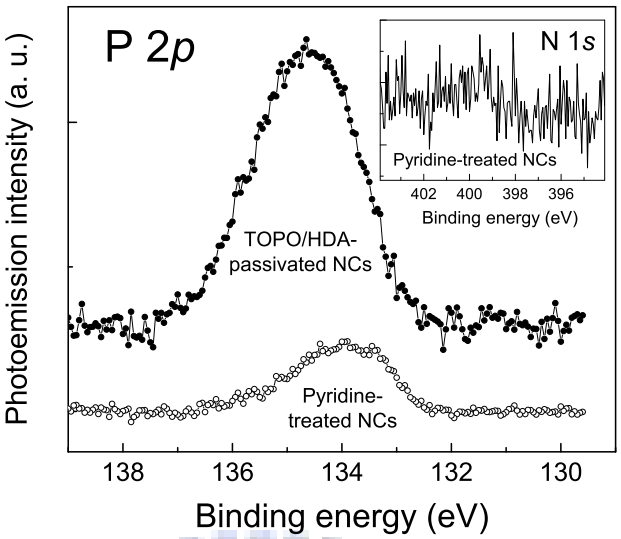

FIG. 4.3: P 2*p* photoemission spectra of CdSe nanocrystals passivated with TOPO/HDA and treated with pyridine. Inset: N 1*s* spectrum of CdSe nanocrystals treated with pyridine.

In order to investigate the effect of surface passivation on the energy shift of CdSe NCs, we changed TOPO/HDA into pyridine as the surfactants with dispersing the NCs in excess pyridine. The organic passivants can be examined by probing the P 2*p* and N 1*s* core-level photoemission spectra since TOPO and pyridine molecules have P and N atoms, respectively. Figure 4.3 shows P 2*p* level spectra, normalized to the intensities of Se 3*d* spectra and incident photon flux, before and after NCs were treated by pyridine. The P 2*p* signal of NCs treated with pyridine was much smaller than that of TOPO/HDA-passivated NCs, indicating that TOPO molecules are effectively displaced; in addition, there is a significant shift towards lower binding energy with respect to that of TOPO/HDA-passivated NCs; this shift may be partially due to some free TOPO molecules without attaching to the NC surface after pyridine treatment. However, we did not detect N 1*s* signal in the spectrum even for NCs treated with pyridine (the inset of Fig. 4.3). This indicates that most pyridine molecules left the NC surface in vacuum, which is also testified in the previous report [17], implying

that the bond strength of Cd−pyridine is weaker than that of Cd−TOPO.

b). Cd $3d_{5/2}$ and Se $3d$ core-level spectra

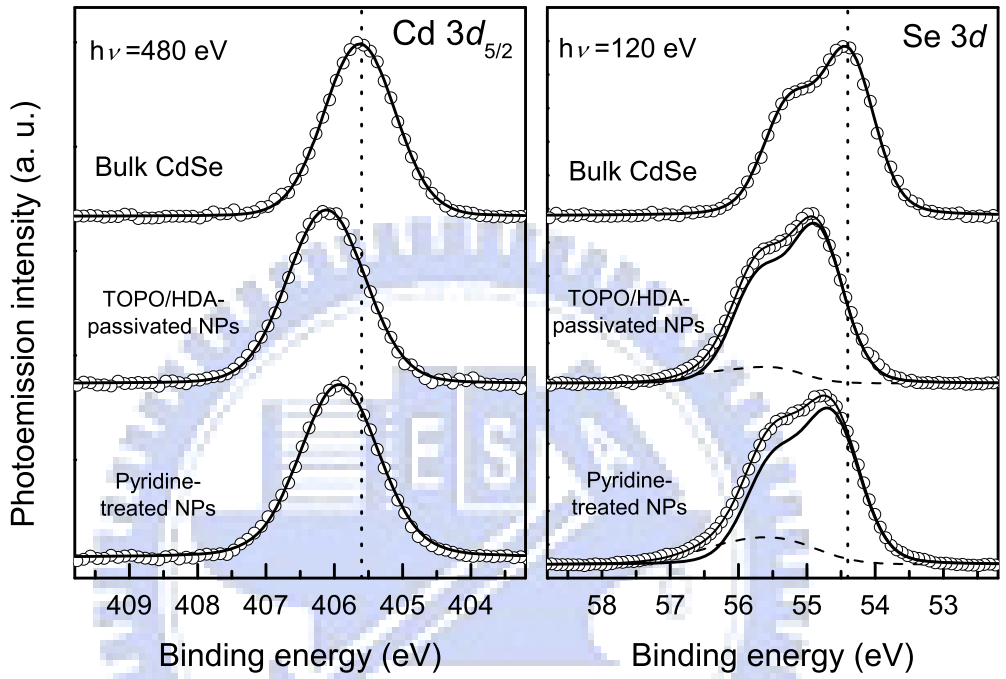

FIG. 4.4: Core-level photoemission spectra of bulk CdSe and CdSe nanocrystals of mean diameter (D_m) of 32 Å, passivated with TOPO/HDA and treated with pyridine. (a) All Cd $3d_{5/2}$ spectra are satisfactorily fitted with a single Voigt component. (b) Se $3d$ spectra are composed of interior (thick solid curves) and surface (dashed curves) components except for bulk CdSe. The binding energies of the Cd $3d_{5/2}$ and Se $3d_{5/2}$ spectra of bulk sample are indicated.

As shown in Fig. 4.4, NCs treated with pyridine have a smaller energy shift of either Cd $3d_{5/2}$ sublevel or Se $3d$ level photoemission spectra compared to NCs passivated with TOPO/HDA. Though the energy shift of NCs treated with pyridine is small, it is still significant. It is noticeable that the intensity of the surface component (at higher binding energy) for NCs treated by pyridine is larger than that for NCs passivated with TOPO/HDA. The reason could be that

the former has more unpassivated Se atoms at the NC surface and/or a rougher surface.

c). Valence-band spectra

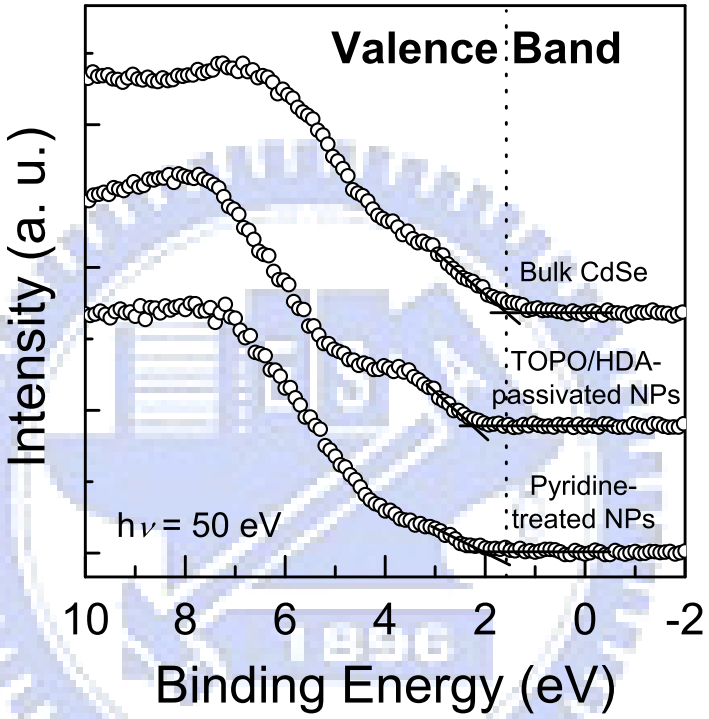

FIG. 4.5: Photoemission spectra in the valence-band binding-energy regime of bulk CdSe and CdSe nanocrystals with mean diameter of 32 Å passivated with TOPO/HDA and treated with pyridine.

Figure 4.5 reveals valence-band photoemission spectrum of CdSe NCs treated by pyridine, of mean diameter 32 Å, together with those of TOPO/HDA-passivated NCs and bulk CdSe. NCs treated with pyridine possess a spectrum in the valence-band range similar to that of NCs passivated with TOPO/HDA, but have a smaller shift of the valence-band edge. We note that the

first feature just below the valence-band edge for NCs treated with pyridine is less apparent than that for NCs passivated with TOPO/HDA despite they have the same size, which is probably influenced by different surface states.

4.3 Photoemission final-state effect

According to a three-step model of photoemission, an electron is excited to an unoccupied state leaving a hole; this photoelectron travels to the surface and crosses into vacuum. An electrostatic interaction arises between the outgoing photoelectron and the system left behind, and between the hole and its surrounding medium. The kinetic energy of the outgoing photoelectron is a sum of the photon energy and the total system energy of the initial neutral ground state minus the total system (potential) energy of the final hole state.

Here we consider a classical electrostatic model. Assuming a point charge q at point $\vec{r}_q$ inside a dielectric sphere with a dielectric constant ε embedded in vacuum, we solve the electrostatic boundary-value problem at the interface yielding the total potential at point $\vec{r}$ also inside the sphere as

$$\phi_{in} = \frac{q}{\varepsilon}\frac{1}{\left|\vec{r}-\vec{r}_q\right|} + \frac{q}{R}\left(\frac{\varepsilon-1}{\varepsilon}\right)\sum_{k=0}^{\infty}\frac{k+1}{k(\varepsilon+1)+1}\frac{r_q^k}{R^{2k}}r^k P_k(\cos\theta), \qquad (4.1)$$

in which R is the spherical radius, P_k is a Legendre polynomial, and θ is the angle between $\vec{r}$ and $\vec{r}_q$. The first term is due directly to the point charge while the second term is due to its image, or the induced polarization of the dielectric host because its size is finite. The corresponding potential outside the dielectric sphere is

$$\phi_{out} = q\sum_{k=0}^{\infty} \frac{2k+1}{k(\varepsilon+1)+1} \frac{r_q^k}{r^{k+1}} P_k(\cos\theta), \tag{4.2}$$

this form ensures that the potential vanishes at infinity. Details of the derivation are given in Appendix B.

If the photoelectron travels to infinity, there is no interaction between the photoelectron and the remaining system with a photohole. The energy of the final state is the energy between the photohole and its image. According to Eq. (4.1) and after rearrangement to facilitate numerical computation, we express the final-state energy as

$$E_f(R, r_h) = \frac{e^2}{2R}\left(\frac{\varepsilon-1}{\varepsilon}\right) + \frac{e^2}{2R\varepsilon}\left(\frac{\varepsilon-1}{\varepsilon+1}\right)\frac{r_h^{\,2}}{R^2 - r_h^{\,2}} + \frac{e^2}{2R}\left(\frac{\varepsilon-1}{\varepsilon+1}\right)\sum_{k=1}^{\infty} \frac{1}{k(\varepsilon+1)+1}\left(\frac{r_h}{R}\right)^{2k}, \tag{4.3}$$

in which r_h is the position of the photohole residing in the particle; the factor one half denotes the self energy or the integration of q from 0 to e. Brus formulated an identical expression as the loss of dielectric solvation energy [18]. In the limit of a large particle or the bulk ($R \to \infty$), the first term vanishes. The second term approaches $e^2/(4h)\{(\varepsilon-1)/[\varepsilon(\varepsilon+1)]\}$ for $r_h = R - h$, which is the correct form of image potential at a planar surface. The third term also vanishes as the series approaches $ln(R)$.

4.4 Discussion

4.4.1 *Energy shift of TOPO/HDA-passivated CdSe nanocrystals*

a). Core-level shift

As there is no electrostatic energy in the initial neutral ground state, the measured binding-energy shift of the core levels with respect to bulk becomes

$$\Delta E_{CL}(R,r_h) = E_f(R,r_h) - E_f(\infty,r_h)\,. \tag{4.4}$$

The energy of the final state defined here arises because the organic ligands (TOPO and HDA molecules), with long carbon chains, that passivate the NC surfaces to prevent the photohole from becoming neutralized by an electron tunneling from the metallic substrate before the photoelectron escapes far [19]. The bulk CdSe powder sample was, however, not isolated and the photohole was readily neutralized from an electron at the Fermi energy during the photoemission. The associated energy of the final state is thus expected to be minimal, which in the following analysis allows us to take that energy as zero in the bulk limit. The practice justifies this assumption as we subsequently discuss. In the metallic limit as $\varepsilon \to \infty$, the energy of the final state approaches $e^2/(2R)$, the classical charging energy.

In photoemission spectroscopy the primary electron signal becomes attenuated through inelastic scattering as it travels through the interior and then escapes from the surface. The measured energy shift is related to the position of the photohole weighted with an exponential factor describing that attenuation,

$$\Delta E_{CL}(R) = \frac{\int_0^{R-\delta} r^2 dr \cdot \int d\Omega \cdot E_f(R,\vec{r}_h) \cdot e^{-\ell(\vec{r}_h)/\lambda(E_{kin})}}{\int_0^{R-\delta} r^2 dr \cdot \int d\Omega \cdot e^{-\ell(\vec{r}_h)/\lambda(E_{kin})}}, \tag{4.5}$$

in which δ denotes the thickness of the surface region not included in the integration, ℓ is the distance for the photoelectron to travel through the dielectric along the normal direction of emission from the position $\vec{r}_h$ of a photohole below the surface, and λ is the inelastic mean free path (IMFP)

depending on the kinetic energy of the photoelectron. The integration is performed over the whole spherical particle. We consider the surface atoms to be located within half a wurtzite lattice parameter a_w (~4.3 Å), which has been used to simulate the diffraction of CdSe NCs on surface relaxation [20]. The IMFP is determined according to the "TPP-2M" formula proposed by Tanuma, Powell and Penn [21]; the physical parameters involved in this formula are the density of the solid, the number of valence electrons per atom or molecule, the atomic or molecular mass and the energy of the band gap. We used 4.66 Å for an IMFP of CdSe obtained with a photoelectron kinetic energy about 60 eV.

Figure 4.6(a) plots the measured energy shifts, dependent on size, relative to the bulk for Cd $3d_{5/2}$ and the interior component of Se $3d$ core-level spectra of CdSe NCs passivated with TOPO/HDA compared with a calculation (solid curve) according to Eq. (4.5), in which the values of the high-frequency dielectric constant ε of CdSe NC dependent on size [$\varepsilon_{bulk}(\infty) = 6.2$] are obtained from the literature [22]. The horizontal error bars specify the full width at half maximum of the size distribution of CdSe NCs, while the vertical error bars indicate the measurement uncertainty. The calculated shifts of the final state without adjustable parameters are in good agreement with the measured energy shifts of the core levels for TOPO/HDA-passivated CdSe NCs with a negligible effect of the final state in the bulk. The magnitude of the Cd $3d_{5/2}$ core-level shift for each size is in general slightly larger than that of the Se $3d$ levels. We attribute this phenomenon to the unresolved Cd $3d$ spectra with the surface Cd contribution that is weighted more to the shift of the final state. To avoid divergence in our classical model, a finite surface thickness δ must be included in Eq. (4.5).

In addition, we undertook a simplified model calculation by considering an effective photohole position $r_h = R - h$ as the fitting parameter for the experimental data; the result is plotted as the dashed curve in Fig. 4.6(a) for comparison. A slightly poorer fit than through use of Eq. (4.5) is obtained with $h = 3.6$ Å. This value is reasonable, since it is close to the IMFP of 4.66 Å. The simpler model for an effective photohole position provides a satisfactory approximation to the more complicated spherical IMFP model.

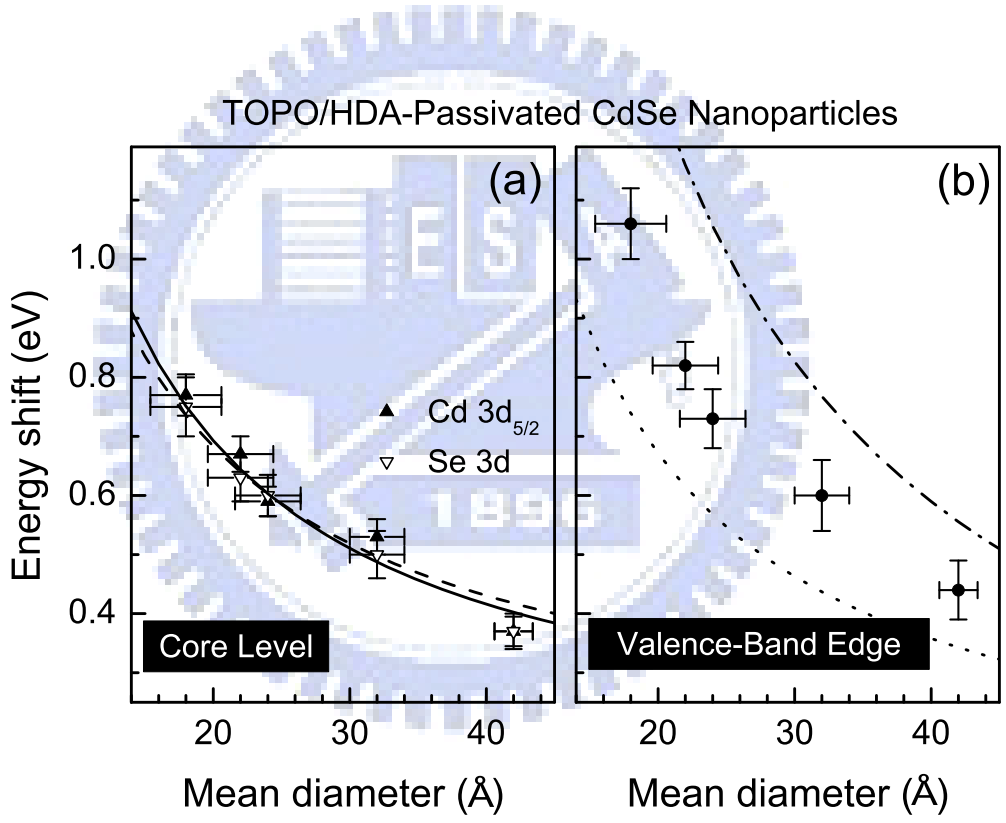

FIG. 4.6: Energy shifts of (a) the core levels and (b) the valence-band edge for CdSe nanocrystals as a function of the mean diameter, compared with model calculations. (a) The solid curve is the shift calculated with Eq. (4.5) with the position of the photohole weighted by an exponential function describing attenuation; the dashed curve is overplotted according to a simplified model with an effective photohole position ($r_h = R - h$) for comparison. (b) The dotted curve indicates the calculated final-state shift weighed with the 1*S* wave function considering the inelastic mean free path, and the dotted-dashed curve includes an additional quantum shift [Eq. (4.7)] reported in Ref. 18.

Using the same parameters, we calculated the bulk term $E_f(\infty, r_h)$ considering the IMFP to be 0.088 eV, which would yield a constant downward shift of the calculated curve in Fig. 4.6(a), apparently deviating from the measured energy shift. If one retains the bulk term while treating the IMFP and the surface thickness as fitting parameters, the resulting fit is much poorer and has an unrealistically large IMFP and an unphysically small surface thickness. Including the bulk term in the effective photohole position model results in a poor fit with an unrealistic photohole position $r_h = R - 0.8$ Å. These results support our assumption to neglect the bulk effect in the final state.

b). Valence-band edge shift

The measured shifts of the valence-band edge of CdSe NCs passivated with TOPO/HDA are presented in Fig. 4.6(b), which is invariably larger than the core-level shift. The final-state shift of the valence-band edge is expected to differ from that of the core levels because the wave function of the valence-edge hole penetrates more deeply into the interior of the NC [22]. Following Ref. 18, we model the hole 1*S* wave function with, for simplicity, $\sin(\pi r/R)/r$ as in an infinite well. This approximation was also used in Ref. 22 to obtain the dielectric constant and exciton energy. The average shift of the final state with the same IMFP is shown as the dotted curve. For a step well the hole wave function is expected to have greater weight near the surface. The pure effect of the final state evidently underestimates the valence-band edge shift. We expect an additional shift due to quantum confinement as the effect of the initial state. The simplest form is the kinetic-energy term in a quantum-confinement well as

described by Brus [23], which has been used with qualitative success to explain the shift in CdS NCs [1]. Wang and Zunger calculated the electronic structure of surface-passivated wurtzite CdSe quantum dots using a semiempirical pseudopotential method (SEPM) [22]; they showed that the valence-band maximum shifts to smaller energy relative to bulk CdSe as the NC becomes smaller.

A correct description of the total shift of the valence-band edge with particle size includes shifts for both the initial and final states as

$$\Delta E_{VB} = \Delta E_{SEPM}(R) + \overline{\Delta E_f(R)}, \tag{4.6}$$

in which $\Delta E_{SEPM}(R)$ is extracted from the predicted energy shifts with size by SEPM [22] and $\overline{\Delta E_f(R)}$ is the average of Eq. (4.3) over the 1*S* wave function of the hole in the particle considering the IMFP [1,18]. The dotted-dashed curve in Fig. 4.6(b) is the plot of Eq. (4.6) using the wave function for an infinite well; it appears to overestimate the measured shifts, and this overestimate becomes worse for smaller NCs. We emphasize here that the amount of the shift for the final state differs in the core levels and the valence-band edge such that to extract the shift of the initial state dependent on size or the quantum confinement by simply subtracting the core-level shift from the valence-band edge shift can yield an underestimate for the larger NCs [12]. Including the IMFP in the calculation of the shift for the valence-band final state produces a minute increase about 0.02 eV, thus a simpler calculation without it is sufficient.

4.4.2 *Energy shift of pyridine-treated CdSe nanocrystals*

a). Dynamic final-state effect

The CdSe NCs treated with pyridine reveal the smaller energy shifts in core levels and valence-band edge compared to TOPO/HDA-passivated NCs (cf. Figs. 4.4 and 4.5). The change in energy shift can be related to the interaction between the NC and its neighbors: TOPO and HDA molecules with long carbon chains that are attached to the NC surface via their lone pairs can prevent the particles from being in contact. In contrast, pyridine is unstable to adsorption on the NC surface in vacuum, leaving the NC partially uncovered with a smaller distance between the NC and the metallic substrate and between the NCs themselves. We expect that the coupling in the latter system is stronger than that in the former, resulting in a higher probability of electron tunneling and a shorter lifetime of the remaining photohole in the particle.

Dynamic effect on a femtosecond time scale has been known for metallic cluster-substrate interactions [5,10,11]. We introduce the dynamic concept in the photoemission final state, i.e., the photohole becomes neutralized while the photoelectron is still in a region near the NC surface before it escapes far or to infinity, to elucidate the observed energy shifts of NCs treated with pyridine.

A schematic diagram describing the effect of a dynamic final state is illustrated in Fig. 4.7, in which is drawn the electrostatic potential energy of the photoelectron as a function of its position outside the dielectric sphere. The zero potential energy is defined as the photoelectron approaches infinity. In the presence of the photohole, the potential energy is the sum of contributions from the induced image and the photohole following the solid curve. If the photohole becomes neutralized when the photoelectron travels to $R+v\tau$, the potential energy of the photoelectron transfers to the dashed curve as only the image potential energy remains. Work needed to be done to remove the photoelectron to infinity is thus decreased by the interaction energy of the electron and hole,

deduced from Eq. (4.2),

$$E_{e-h}(R,\vec{r}) = \frac{e^2}{|\vec{r}_e - \vec{r}_h|}\left(\frac{2}{\varepsilon+1}\right) + \frac{e^2}{r_e}\left(\frac{\varepsilon-1}{\varepsilon+1}\right) + \frac{e^2}{r_e}\left(\frac{\varepsilon-1}{\varepsilon+1}\right)\sum_{k=1}^{\infty}\frac{1}{k(\varepsilon+1)+1}\left(\frac{r_h}{r_e}\right)^k P_k(\cos\theta), \tag{4.7}$$

in which $\vec{r}_e = \vec{R} + \Delta\vec{r}$ with $\Delta\vec{r} = \vec{v}_\ell \tau$, $\vec{v}_\ell$ is the velocity of the photoelectron towards the analyzer, and θ is the angle between $\vec{r}_e$ and $\vec{r}_h$. In this model, for simplicity we take τ as an average relaxation time instead of the characteristic time in the tunneling probability used in Ref. 5. In consequence, the total energy shift of photoemission core-level spectra based on the dynamic final-state effect is given by

$$\Delta E_{CL}^{dyn}(R,\vec{r}) = \Delta E_{CL}(R) - E_{e-h}(R,\vec{r}). \tag{4.8}$$

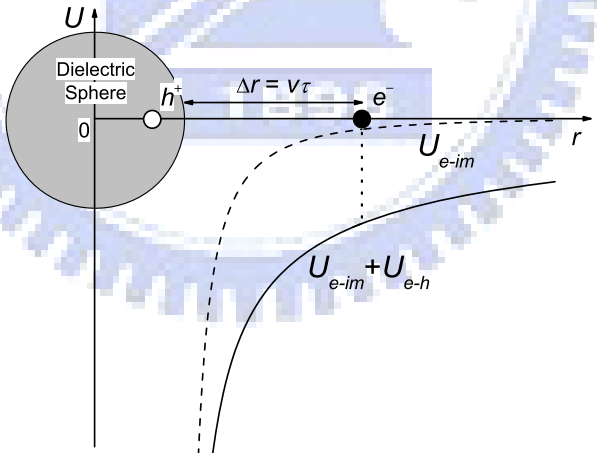

FIG. 4.7: Schematic diagram of the dynamic final-state effect illustrates the electrostatic potential-energy curve as the photoelectron travels to infinity at which the zero energy is defined. In the presence of the photohole, the potential energy is the sum of the electron-hole energy ($U_{e\text{-}h}$) and the electron-image energy ($U_{e\text{-}im}$) following the solid curve. If the photohole becomes neutralized when the photoelectron travels to $R + v\tau$ the potential energy transfers to the dashed curve as only the electron-image energy remains.

When the dielectric constant approaches infinity, this leads to $\lim_{\varepsilon\to\infty}\left[\Delta E_{CL}^{dyn}(R,r)\right]=e^2\left[1/(2R)-1/r\right]$, closely resembling a model proposed for metallic clusters on a graphite substrate [5].

b). Core-level shift

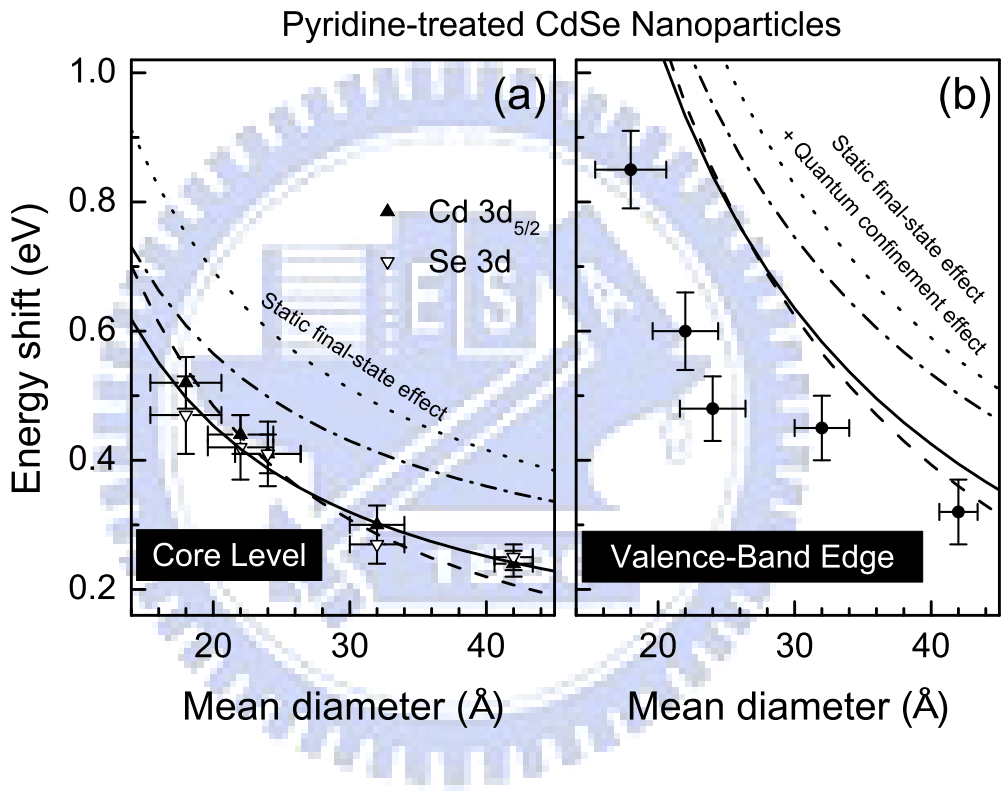

FIG. 4.8: Energy shifts of (a) the core levels and (b) the valence-band edge for CdSe nanocrystals treated with pyridine as a function of the mean diameter, compared with model calculations. (a) The dashed curve is the calculation based on a model for a dynamic effect in the final state that takes into account the lifetime of the photohole. The solid and dotted-dashed curves include the contribution from the nearest-neighboring particles with and without considering the dynamic effect in the final state, respectively. (b) The dashed curve results from a calculation based on a model for the dynamic effect in the final state with the same parameter used in Fig 4.8(a). The solid and dotted-dashed curves specify the total shift including the contribution from the nearest-neighboring particles with and without the dynamic final-state effect, respectively.

A fit of Eq. (4.8) to the core-level energy shifts of CdSe NCs treated with pyridine is shown in Fig. 4.8(a) as the dashed curve. The experimental results are satisfactorily described with our model with a parameter $\Delta r = 68$ Å. This means that the outgoing photoelectron maintains an interaction with the photohole left behind in the particle until it travels 68 Å from the surface. The photoelectron leaves the NC with a kinetic energy about 60 eV for the Se 3*d* level, corresponding to a velocity $\bar{v}_\ell = 4.6\times10^6$ m/sec. The lifetime of the photohole left in the dielectric particle is thus $\tau = 1.48\times10^{-15}$ sec, but the smallest and largest NC data show a perceptible deviation from the model fitted curve (dashed curve).

We further consider the influence of the nearest-neighboring particles as a correction because the interparticle distances were small for NCs treated with pyridine (see Fig. 2.4). An additional interaction between the remaining photohole and the induced image charges in the neighboring NCs can diminish the apparent energy shift in the final state. The TEM images showed an arrangement of nearly hexagonal close-packed NCs. We estimate from, for example, Fig. 2.4 that, on average, one NC in the surface layer of a film had four neighboring NCs nearly in contact, but maintained a distance ~15 Å surface to surface from the other five nearest neighbors, because of remaining TOPO/HDA surfactants on the NC surface [17,24]. For simplicity we assume that the remaining photohole was effectively located at the center of the NC and interacted with the induced image charges of all nearest-neighboring NCs. The final-state shift after this correction for the nearest neighbors is shown as the dotted-dashed curve in Fig. 4.8(a). An additional decrease is clearly required, which is again due to the dynamic effect in the final state. The best fit including

both the dynamic effect in the final state and the correction for the nearest neighbors is plotted as a solid curve in Fig 4.8(a), showing good agreement with data points of all sizes. In this fit, $\Delta r = 128$ Å or $\tau = 2.78\times10^{-15}$ sec. This value is expected to correspond to the upper limit of the lifetime, as most photoholes are created near the NC surface leading to a smaller contribution from neighboring particles than our assumption at the center. The interaction between photoelectron and image becomes small for $\Delta r > 30$ Å, because of its dipolar character, and is almost negligible in the above-mentioned dynamic effect and the correction due to nearest neighbors. For NCs passivated with TOPO/HDA, the mean distance surface to surface between NCs was ~15 Å. The energy shifts, for the particle size ranging from 42 to 18 Å, are thus decreased by 0.02−0.04 eV considering the contribution from the neighbors, which is insignificant to affect our conclusion.

c). Valence-band edge shift

Figure 4.8(b) shows the valence-band edge shifts of CdSe NCs treated with pyridine compared with the calculation based on the model for a dynamic effect in the final state with the same parameters as for the corresponding core-level shift. We also considered the contribution from the nearest-neighboring particles (dotted-dashed and solid curves). The calculation evidently overestimates the measurement and the deviation is similar to that in Fig. 4.6(b).

Our estimate shows the photohole lifetime to be in a range $1.5-2.8\times10^{-15}$ sec for NCs treated with pyridine. Accordingly the dynamic effect of the final state cannot be ignored for a system with strong interactions between a dielectric particle and a metallic substrate and between particles. For comparison, the

dynamic effect in the final state has been observed in naked Ag nanoparticles [5] and in Ag and Au nanoparticles passivated with alkanethiolate supported on a graphite surface [9-11] with a photohole lifetime $0.2-0.5\times10^{-15}$ sec, smaller than our case.

4.4.3 *Overestimate in the valence-band edge shift*

We find that, for NCs either passivaed with TOPO/HDA or treated by pyridine, the calculated energy shift in the valence-band edge is larger than the experimental data. Several reasons underlie this deviation. One might suspect an approximation of a NC of prolate shape (aspect ratio of 1.1−1.3) by a sphere to result in an error in the initial-state calculation, but the deviation of a prolate spheroid from the averaged sphere invariably produces an increase of quantum confinement and a larger shift in the initial state, contrary to the experimental observation. Another point is the presence of stacking faults in NC that have been experimentally observed [25], but a calculation of CdSe quantum dots in both wurzite and zincblende structures shows no significant alteration of exciton energies [26]. Stacking faults thus seem unable to explain such a discrepancy. A third possibility is that a lattice contraction up to 1 % and structural disorder were observed experimentally [15] while the calculation assumes a truncated bulk with a bulk lattice parameter. According to a theoretical investigation of CdS clusters, the band gap is decreased 0.11 eV assuming 1.4 % lattice contraction [27]. This effect might explain the discrepancy between experiment and theory.

4.5 Summary

We have investigated the energy shift dependent on size of the core levels and valence-band edge for organically passivated CdSe nanocrystals of various diameters. For nanocrystals passivated with TOPO/HDA the core-level shifts are well described with a model of a static final state based on an electrostatic interaction between the photohole and the dielectric background, including the inelastic mean free path effect of the photoelectron, with no adjustable parameter. For nanocrystals treated with pyridine, on the other hand, the energy shifts are smaller. A dynamic model characterizing the finite lifetime of the photohole on a femtosecond scale is invoked to elucidate these energy shifts considering the interaction between photoelectron and photohole. For the valence-band edge an additional shift in the initial state due to quantum confinement is required to explain the data. A pseudopotential calculation of the valence-band edge shift in the literature appears to overestimate the effect in the initial state compared to our experimental observation. The discrepancy might reflect a lattice contraction in the nanoparticle that was neglected in the calculation.

4.6 References

[1] V. L. Colvin, A. P. Alivisatos, and J. G. Tobin, Phys. Rev. Lett. **66**, 2786 (1991).

[2] P. Zhang and T. K. Sham, Phys. Rev. Lett. **90**, 245502 (2003).

[3] G. K. Wertheim, S. B. DiCenzo, and S. E. Youngquist, Phys. Rev. Lett. 51, 2310 (1983).

[4] H. G. Boyen, A. Ethirajan, G. Kästle, F. Weigl, P. Ziemann, G. Schmid, M. G. Garnier, M. Büttner, and P. Oelhafen, Phys. Rev. Lett. **94**, 16804 (2005).

[5] H. Hovel, B. Grimm, M. Pollmann, and B. Reihl, Phys. Rev. Lett. **81**, 4608 (1998).

[6] D. M. Wood, Phys. Rev. Lett. **46**, 749 (1981).

[7] G. Makov, A. Nitzan, and L. E. Brus, J. Chem. Phys. **88**, 5076 (1987).

[8] M. Seidl, K. H. Meiwes-Broer, and M. Brack, J. Chem. Phys. **95**, 1295 (1991).

[9] A. Tanaka, Y. Takeda, T. Nagasawa, and S. Sato, Phys. Rev. B **67**, 33101 (2003).

[10] A. Tanaka, Y. Takeda, M. Imamura, and S. Sato, Phys. Rev. B **68**, 195415 (2003).

[11] M. Imamura and A. Tanaka, Phys. Rev. B **73**, 125409 (2006).

[12] T. van Buuren, L. N. Dinh, L. L. Chase, W. J. Siekhaus, and L. J. Terminello, Phys. Rev. Lett. **80**, 3803 (1998).

[13] S. W. Gaarenstroom and N. Winograd, J. Chem. Phys. **67**, 3500 (1977).

[14] H. Borchert, D. V. Talapin, C. McGinley, S. Adam, A. Lobo, A. R. B. de Castro, T. Moller, and H. Weller, J. Chem. Phys. **119**, 1800 (2003).

[15] K. S. Hamad, R. Roth, J. Rockenberger, T. van Buuren, and A. P. Alivisatos, Phys. Rev. Lett. **83**, 3474 (1999).

[16] E. Agostinelli, C. Battistoni, D. Fiorani, G. Mattogno, and M. Nogues, J. Phys. Chem. Solids **50**, 269 (1989).

[17] J. E. Bowen Katari, V. L. Colvin, and A. P. Alivisatos, J. Phys. Chem. **98**, 4109 (1994).

[18] L. E. Brus, J. Chem. Phys. **79**, 5566 (1983).

[19] If the (insulating) films are too thick, the electron-tunneling time or

photohole lifetime becomes too long compared to the time until the next photoionization event. Macroscopic charging is observed with a large shift proportional to the photon flux. To avoid this unwanted phenomenon, we used a highly dilute solution to prepare thin multilayer films.

[20] M. G. Bawendi, A. R. Kortan, M. L. Steigerwald, and L. E. Brus, J. Chem. Phys. **91**, 7282 (1989).

[21] S. Tanuma, C. J. Powell, and D. R. Penn, Surf. Interface Anal. **21**, 165 (1993).

[22] L. W. Wang and A. Zunger, Phys. Rev. B. **53**, 9579 (1996).

[23] L. E. Brus, J. Phys. Chem. **90**, 2555 (1986).

[24] B. S. Kim, L. Avila, L. E. Brus, and I. P. Herman, Appl. Phys. Lett. **76**, 3715 (2000).

[25] C. B. Murray, D. J. Norris, and M. G. Bawendi, J. Am. Chem. Soc. **115**, 8706 (1993).

[26] B. Zorman, M. V. Ramakrishna, and R. A. Friesner, J. Phys. Chem. **99**, 7649 (1995).

[27] M. V. Rama Krishna and R. A. Friesner, J. Chem. Phys. **95**, 8309 (1991).